

UCLA

UCLA Previously Published Works

Title

Enhancing mitosis quantification and detection in meningiomas with computational digital pathology.

Permalink

<https://escholarship.org/uc/item/6q73c3tx>

Journal

Acta Neuropathologica Communications, 12(1)

Authors

Gu, Hongyan

Yang, Chunxu

Al-Kharouf, Issa

et al.

Publication Date

2024-01-11

DOI

10.1186/s40478-023-01707-6


Peer reviewed

RESEARCH

Open Access



# Enhancing mitosis quantification and detection in meningiomas with computational digital pathology

Hongyan Gu<sup>1</sup>, Chunxu Yang<sup>1</sup>, Issa Al-kharouf<sup>2</sup>, Shino Magaki<sup>3</sup>, Nelli Lakis<sup>2</sup>, Christopher Kazu Williams<sup>3</sup>, Sallam Mohammad Alrosan<sup>2</sup>, Ellie Kate Onstott<sup>2</sup>, Wenzhong Yan<sup>1</sup>, Negar Khanlou<sup>3</sup>, Inma Cobos<sup>4</sup>, Xinhai Robert Zhang<sup>5</sup>, Neda Zarrin-Khameh<sup>6</sup>, Harry V. Vinters<sup>3</sup>, Xiang Anthony Chen<sup>1\*</sup> and Mohammad Haeri<sup>2\*</sup> 

## Abstract

Mitosis is a critical criterion for meningioma grading. However, pathologists' assessment of mitoses is subject to significant inter-observer variation due to challenges in locating mitosis hotspots and accurately detecting mitotic figures. To address this issue, we leverage digital pathology and propose a computational strategy to enhance pathologists' mitosis assessment. The strategy has two components: (1) A depth-first search algorithm that quantifies the mathematically maximum mitotic count in 10 consecutive high-power fields, which can enhance the preciseness, especially in cases with borderline mitotic count. (2) Implementing a collaborative sphere to group a set of pathologists to detect mitoses under each high-power field, which can mitigate subjective random errors in mitosis detection originating from individual detection errors. By depth-first search algorithm (1), we analyzed 19 meningioma slides and discovered that the proposed algorithm upgraded two borderline cases verified at consensus conferences. This improvement is attributed to the algorithm's ability to quantify the mitotic count more comprehensively compared to other conventional methods of counting mitoses. In implementing a collaborative sphere (2), we evaluated the correctness of mitosis detection from grouped pathologists and/or pathology residents, where each member of the group annotated a set of 48 high-power field images for mitotic figures independently. We report that groups with sizes of three can achieve an average precision of 0.897 and sensitivity of 0.699 in mitosis detection, which is higher than an average pathologist in this study (precision: 0.750, sensitivity: 0.667). The proposed computational strategy can be integrated with artificial intelligence workflow, which envisions the future of achieving a rapid and robust mitosis assessment by interactive assisting algorithms that can ultimately benefit patient management.

**Keywords** Mitosis, Meningioma, Depth-first search, Pathologist group decision, Digital pathology

\*Correspondence:

Xiang Anthony Chen

[xac@ucla.edu](mailto:xac@ucla.edu)

Mohammad Haeri

[mhaeri@kumc.edu](mailto:mhaeri@kumc.edu)

Full list of author information is available at the end of the article



© The Author(s) 2024. **Open Access** This article is licensed under a Creative Commons Attribution 4.0 International License, which permits use, sharing, adaptation, distribution and reproduction in any medium or format, as long as you give appropriate credit to the original author(s) and the source, provide a link to the Creative Commons licence, and indicate if changes were made. The images or other third party material in this article are included in the article's Creative Commons licence, unless indicated otherwise in a credit line to the material. If material is not included in the article's Creative Commons licence and your intended use is not permitted by statutory regulation or exceeds the permitted use, you will need to obtain permission directly from the copyright holder. To view a copy of this licence, visit <http://creativecommons.org/licenses/by/4.0/>. The Creative Commons Public Domain Dedication waiver (<http://creativecommons.org/publicdomain/zero/1.0/>) applies to the data made available in this article, unless otherwise stated in a credit line to the data.

## Introduction

Meningioma is the most common primary brain tumor, accounting for approximately 40% of central nervous system (CNS) neoplasms in the United States [1]. According to the 2021 WHO classification of tumors of the CNS, (WHO CNS 5 Blue Book), the mitotic count (MC), calculated in 10 consecutive high-power fields (HPFs,  $1\text{HPF}=0.16\text{mm}^2$ ) from areas of the highest mitotic activity on H&E slides, is one critical criterion for meningioma grading [2]. Nonetheless, pathologists' evaluation of MC varies due to obstacles in pinpointing hotspot areas, first, and detecting mitosis events within these areas [3–5]. Therefore, it is essential to create a more robust solution to ensure a reliable MC assessment for grading of meningiomas, which is important in clinical management and prognosis [6–8].

Besides histologic examination of the H&E slides, immunohistochemistry (IHC) staining has been used to assist with more accurate MC. For example, a proliferation index, derived from Ki-67 IHC, has been employed as a tool to correlate with the mitotic activity [9–11]. However, the Ki-67 proliferation index cannot fully replace the mitotic count, likely due to variation in staining among institutions, subjectivity of percentage assessment, and the absence of a clear threshold cutoff [12]. More recently, other IHCs such as Phosphohistone-H3 (PHH3) immunostains – effective in detecting both G2 and mitosis phases [13] – proved to be a reliable indicator for mitosis reading [14–17]. However, the PHH3 is not an acceptable criterion in the WHO criteria and thus, is mainly used in research studies.

It is noteworthy that the WHO CNS 5 Blue Book has incorporated molecular alterations as an alternative pathway for diagnosing grade 3 meningiomas, described as harboring a *TERT* promoter mutation and/or homozygous loss of *CDKN2A/B* [2]. Recent works on methylation profiling can also classify grade 3 meningiomas [18]. However, there are no clear molecular criteria for the majority of WHO 1 and 2 meningiomas, which constitute over 97% of meningiomas [1]. While the current WHO CNS guideline may not be the best predictor of tumor outcome, it is still not clear whether DNA copy number analysis, methylation profiling, or other factors are the better predictor of tumor recurrence and aggressive behavior [19–22]. Further investigation in methylation profiling and other molecular alterations along with clinical studies are still required to correlate with new approaches of tumor grading and classification.

As of 2023, histologic examination and evaluation of mitotic activity by pathologists still remain an important element for meningioma grading, considering its cost effectivity. However, this process is prone to a high level of variation because of two factors: (1) lack

of standardized protocols for selecting 10 consecutive HPFs, resulting in differences in evaluated areas [3, 23]; and (2) inconsistencies in detecting mitosis within the selected 10 HPFs, stemming from controversy in mitosis verification, the small size, often low prevalence in grade 1 and most of grade 2 tumors, and heterogeneous distribution of mitotic figures [4, 5, 24].

The recent advancements in digital pathology and artificial intelligence (AI) technologies have shown promise in assisting pathologists in mitosis examination: A study of Aubreville et al. demonstrated that AI could outperform pathologists in localizing mitotic hotspots from digitized pathology slides [23]. AI-assisted systems have been developed to calculate and recommend hotspots equivalent to 10 consecutive HPFs for pathologists [25, 26]. The use of AI can save pathologists' effort in searching for mitoses under high magnification, leading to improved sensitivities [25, 27], agreement rates [28], and confidence [26] in identifying mitotic figures. However, the current AI approaches have two major limitations:

1. AI-assisted systems typically calculate mitosis hotspots as circle [29], square [25] or rectangular [26, 27, 30, 31] regions, which may not completely align with the actual distribution of mitosis in tumors. As a result, the number of mitoses included in these recommended hotspot areas might be fewer, as the morphology of these hotspots lacks flexibility and nuance.
2. The current mitosis AI is trained on data from limited sources, such as specific patients, hospitals, and scanners [30–33]. Consequently, the AI may not achieve optimal performance when confronted with new and diverse data [34–36]. The pathologists performing histological analysis are still indispensable under such situations.

This work overcomes the limitations of current computational methods for mitosis quantification and detection by introducing a strategy that harnesses the preciseness of the computer algorithm and the collective intelligence of human pathologists. The first element of the strategy aims to enhance quantification, consisting of a computer algorithm called “depth-first search” (DFS). It can calculate the mathematically maximum possible MC in 10 consecutive HPFs of a slide, along with their corresponding locations. By analyzing 19 fully-annotated meningioma slides, we demonstrate that the DFS algorithm can identify 4.29 more and 3.32 more mitoses in 10 consecutive HPFs on average, compared to mitoses counted in linear and rectangular HPF arrangements, respectively. As a result, the elevated mitoses counted by the proposed DFS algorithm led to potential upgrades

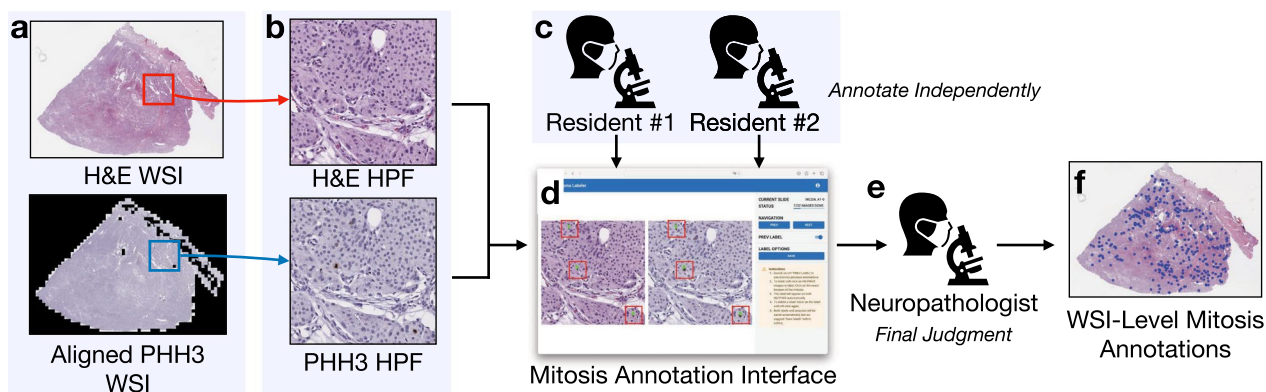


**Fig. 1** Workflow for mitosis annotation. **a** H&E and aligned PHH3 WSIs were prepared. **b** H&E and PHH3 image tiles with a size of one HPF were cut from corresponding WSIs. **c** Two pathology residents annotated mitoses on H&E-PHH3 HPF tiles independently using **d** the mitosis annotation interface. **e** A neuropathologist reviewed mitosis annotations from the two pathology residents and provided the final judgment for each one. **f** Mitosis annotations were transferred onto H&E WSIs for further analysis (each dot represents a mitosis annotation)

of two cases compared to the previous diagnoses verified by consensus conferences. The second element of the computational strategy targets to improve mitosis detection by leveraging the collective expertise of a group of pathologists. This approach involves letting a certain number of pathologists annotate mitoses independently and generating a final judgment through a majority vote. To validate this element, we hosted a user study involving 41 pathologists and pathology residents, where each participant independently annotated mitoses based on their own judgments in 48 selected HPFs of meningiomas. We evaluated the correctness of annotations from each participant, as well as the majority voting decisions generated from randomly-sampled subgroups. We report that groups of three pathologists and/or pathology residents can achieve an average precision of 0.897 and sensitivity of 0.699 in mitosis detection, which is higher than an average pathologist, who had a precision of 0.750 and a sensitivity of 0.667.

## Materials and methods

### Meningioma specimen preparation and mitosis annotation

All specimens were collected from the department of Pathology and Laboratory Medicine, University of California, Los Angeles. A total of 22 slides were selected based on the size of the tissue on the H&E slide and the availability of the corresponding Ki-67 IHC slide. These slides were from 12 patients (6 males, 6 females, age range between 39 and 79 years), including two WHO grade 1, six WHO grade 2, and four WHO grade 3 meningiomas. The grade 2 and grade 3 tumors for each slide were based on mitotic counts. Other criteria for upgrading to a grade 2 or 3 tumor were absent. None of these cases had available molecular testing such as *CDKN2A/B*

and/or *TERT* promoter status. The specimens were collected between October 2019 and December 2021. The formalin fixed paraffin embedded blocks were sectioned at  $6\mu\text{m}$  thickness and stained with H&E followed by whole slide scanning (at  $400\times$  total scanning resolution with a  $20\times$  objective; Leica Aperio CS2). The same slide was then destained and immunostained with PHH3 antibody (1:200, Cell Marque, 369A-16) followed by rescanning of the slide with the same settings used in the first scan.

A two-step image transform approach was used to align PHH3 and H&E whole slide images (WSIs) to assist pathologists in verifying mitoses on H&E. All image alignment procedures were performed on PHH3 WSIs, while the H&E slides remained unaltered. Of the 22 pairs of WSIs, the H&E WSI from one pair was mainly out-of-focus, and two pairs failed to align the PHH3, leaving the remaining 19 WSIs for further annotation (Fig. 1(a)).

H&E and PHH3 image tiles with a size of one HPF (size= $1600 \times 1600$  pixels, or  $0.4\text{mm} \times 0.4\text{mm} = 0.16\text{mm}^2$ )<sup>1</sup> were extracted from WSIs without overlapping (Fig. 1(b)). Two postgraduate year 3 (i.e., three years in training) pathology residents independently annotated the mitoses in each HPF using a web-based interface (Fig. 1(c-d)), which can show H&E and PHH3 HPFs side-by-side. The resident-annotated images were then reviewed by a neuropathologist (M.H.) with the same annotation interface. The neuropathologist provided the final judgment on the mitosis annotation

<sup>1</sup> This work defines an HPF as a square. All HPFs mentioned in this work had sizes of  $0.16\text{mm}^2$ , as defined in the 2021 WHO CNS 5 Blue Book [2]. Therefore, the edge of an HPF was  $0.4\text{mm}$ , or 1,600 pixels ( $0.25\mu\text{m}/\text{pixel}$  for  $400\times$  scans).



using the criteria specified in Additional file 1, Section 1 (Fig. 1(e)). The resulting annotations were transferred to H&E WSIs (Fig. 1f) and were used for the MC analysis.

#### Quantification of the hotspot mitosis count of WSIs

In each of the 19 annotated WSIs from Sect. 2.1, the MC in 10 HPFs was quantified with the following six different methods. Methods 1 – 3 count MCs in consecutive 10 HPFs and are compatible with the current definition of WHO CNS 5 Blue Book, while the HPFs in methods 4 – 6 are not necessarily connected. Background and out-of-focus regions were identified by a deep-learning algorithm [37] and were excluded. Non-tumor regions were marked by a neuropathologist (M.H.) with Aperio ImageScope software (version 12.3.2.8013)<sup>2</sup> and were not used for calculation.

1. *MC in 10 HPFs generated by depth-first search algorithm (Proposed)* This method arranges HPFs as a sequence of 10 connected HPFs that form a *connected* path. Because the HPF view in digital pathology is square, two HPFs that share at least one connected edge are considered connected. The path should be traversed from the first HPF to the tenth, with the requirement that each HPF is visited exactly once. The path is calculated by our proposed DFS algorithm (see Appendix A for implementation), which consists of a recursive depth-first searching with backtracking. In a WSI, the algorithm comprehensively searches all possibilities of 10 connected HPF paths, satisfying the constraint mentioned above to guarantee that the resulting quantification of MC is the highest, mathematically.
2. *MC in linear 10 HPFs* This method quantifies the highest MC of 10 HPFs with the linear arrangement. The highest MCs in  $10 \times 1$  HPFs (vertical) and  $1 \times 10$  HPFs (horizontal) are reported.
3. *MC in rectangular 10 HPFs* This method follows the previously reported algorithm [26] and quantifies the highest MC of 10 HPFs with the rectangular arrangement. The highest MCs in  $5 \times 2$  HPFs (vertical) and  $2 \times 5$  HPFs (horizontal) are reported.
4. *Average MC per 10 HPFs* This method quantifies the average number by dividing the total MC in tumor areas by the size of the tumors and multiplying by 10.
5. *MC in random 10 HPFs* This method [7] randomly samples 10 HPFs from each WSI 1,000 times (without replacement). The distribution of MCs in each set of 10 sampled HPFs is reported.
6. *MC in maximum 10 (not connected) HPFs* The MC of each HPF in the entire WSI is ranked in descending order, and the MC of the top 10 HPFs is added together. This method represents the maximum possible MC that can be observed in 10 HPFs within a WSI.

Furthermore, the MCs yielded by methods 1 – 3 were compared to the WHO grades determined by the consensus conferences. Here, we sought cases where *upgrades* in WHO grades could be according to the criterion of the MC alone.

#### User study for evaluating pathologists' mitosis detection

A user study was conducted to evaluate the ability of pathologists and pathology residents to detect mitoses in meningioma at the magnification comparable to 1 HPF. The study was approved by the Institutional Review Board of the University of California, Los Angeles (IRB#21-000139) and was conducted between February 2023 and May 2023.

Forty-eight images, each equal to 1 HPF surface area, were selected by a neuropathologist (M.H.) from two H&E WSIs of meningotheial-transitional meningioma for each case (see Fig. 2(a) for example), based on five criteria (see Additional file 1, Section 2). Random sampling was not used because approximately 89.1% of the area in the two WSIs did not include mitosis. The decision to limit the number of images to 48 was motivated by practical considerations: our preliminary finding suggested that annotating these 48 HPF images required about 30 min for a pathologist, and increasing the number further would not have been feasible due to the potential risk of causing fatigue among the participants.

Amongst 48 selected HPF images, eight did not include mitoses, while the remaining images had 88 mitoses, ranging from one to six per image. Note that the image set was skewed towards HPFs with one or more mitoses to observe pathologists' correctness when detecting mitoses with various morphologies.

The participants were recruited by sending email invitations to the mailing list and snowball recruitment. In total, 41 participants from 11 institutions (Appendix B) in the United States (N=40) and Costa Rica submitted their responses, including 19 neuropathologists/neuropathology fellows (AP/NP), 10 pathologists/pathology fellows (AP), and 12 pathology residents.

Each participant was instructed to visit our user-study website with their own laptop or desktop computer with recommended settings. On the website, participants watched an instruction video and were asked to answer multiple-choice questions about their occupation and sub-specialty (if applicable). Afterward,

<sup>2</sup> <https://www.leicabiosystems.com/us/digital-pathology/manage/aperio-imagescope/>

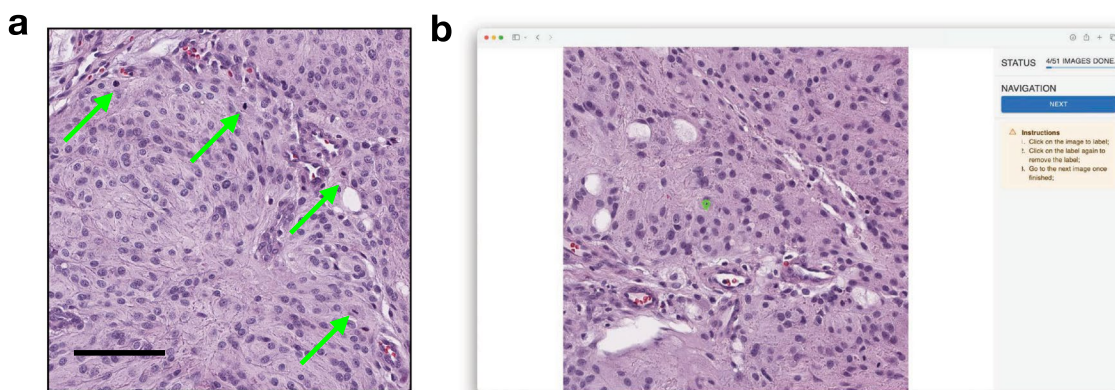


**Fig. 2** **a** Representative HPF image used in the study, with mitoses noted by arrows, bar=100µm. **b** Interface screenshot of the user study website, where the HPF images were shown to participants for mitosis annotation in the random order

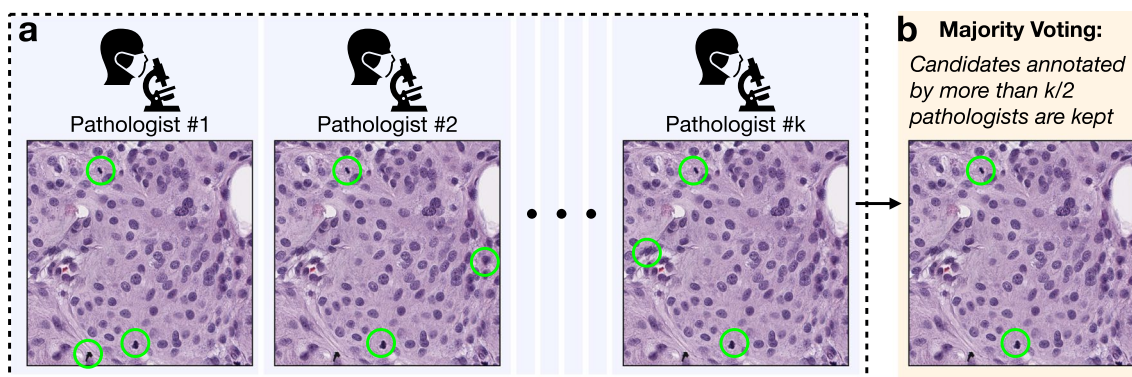


**Fig. 3** Generating mitosis decisions with grouping annotations from a set of  $k$  pathologists. **a** Step 1 (group member selection): annotations were collected from an odd number of  $k$  pathologists. The  $k$  pathologists are selected randomly. **b** Step 2 (majority voting): candidates annotated by more than  $k/2$  pathologists are kept as the final grouping mitosis decision

they reviewed three tutorial images to become familiar with the website interface and the task. Participants were informed that there may be zero to six mitoses in each of the 48 images and were instructed to annotate mitotic figures based on their daily practice experience. The 48 images were presented to each participant in random order (Fig. 2b). To prevent bias, participants were blinded to the mitosis annotations until they completed the study. Their annotations, survey responses, and time logs were recorded for further analysis.

### Grouping pathologists' annotations

The grouping process is based on the participants' annotations collected in Sect. 2.3: First, annotations from an odd number of  $k$  pathologists were randomly selected (Fig. 3(a)). Second, mitosis candidates that were annotated by more than  $k/2$  (i.e., > 50%) participants were kept as the decision of the group (Fig. 3(b)). This approach assigns equal importance weight to each selected participant and emulates a majority voting process. As for the

group size, we randomly selected from the 41 participants without replacement and explored the group size from 3 to 37 (i.e., 3,5,7,9,..., 37). For each group size, we ran the grouping process 100 times for result evaluation.

### Measurements and statistics

The correctness of mitosis detection was measured by precision or positive predictive value (PPV, see Eq. 1) and sensitivity (recall, see Eq. 2), which was calculated according to the true-positive (TP), false-positive (FP), and false-negative (FN) counts. A TP indicates a mitosis present within  $15\mu\text{m}$  (60 pixels) distance of a participant's annotation. An FP stands for no mitoses present within  $15\mu\text{m}$  radius distance of a participant's annotation. And an FN means no participant's annotations present within  $15\mu\text{m}$  radius distance of a mitosis.

We report the precision and sensitivity of three conditions: (1) individual participant; (2) decisions from groups that have sizes between 3 to 37; and, (3) an EfficientNet-b3 Convolutional Neural Network AI model

[38, 39] trained from a part of mitosis annotations collected in Sect. 2.1 (see Additional file 1, Section 3 for the training detail), as a reference. A bootstrapping method (10,000 times, 100% re-sampling with replacement) was used to describe the average and 95% confidence interval for these criteria. For AI evaluation, we ran the AI on the 48 HPF images 100 times. In each test run, these HPF images were randomly flipped and/or rotated ( $0^\circ, 90^\circ, 180^\circ, 270^\circ$ ), and the Dropout layers in the AI model were enabled.

$$\text{Precision}(PPV) = \frac{TP}{TP + FP} \quad (1)$$

$$\text{Sensitivity (Recall)} = \frac{TP}{TP + FN} \quad (2)$$

We further tested whether participants' precision and sensitivity varied according to their experience level: a Kruskal-Wallis Test was applied to test significance among three of the participants' experience levels (i.e., AP/NP, AP, and pathology residents). A post-hoc Dunn's test was used to show pair-wise difference between each experience level.

Finally, we introduced a metric called *agreement rate* as a measure of participants' consistency in detecting mitoses: Given a nucleus, its agreement rate was defined as the percentage of participants that annotated it. We calculated the agreement rates for (1) all "ground truth" mitoses (i.e., annotated by the participants in Sect. 2.1), and (2) false-positive mitoses where *more than three* participants agreed on to illustrate false-positive errors with higher agreement rates.

The image processing, AI inferencing, and statistics were performed in a local server with Intel W-2195 CPU with 128GB RAM and Nvidia RTX 3090 Graphics Processing Unit. The server has a Python 3.6.8 environment, with Numpy version 1.19.5, OpenCV version 4.5.2, scikit-image version 0.17.2, scipy version 1.7.3, scikit-learn version 1.0.2, PyTorch 1.12.0, and Matplotlib version 3.5.2 for figure making.

## Results

### Mitosis count in meningioma WSIs

A total of 4,133 mitotic figures were annotated with examples shown in Fig. 4(a). The 19 WSIs exhibit a wide range of total MCs, spanning from 8 to 623 per slide. Figure 4(b) presents the hotspot MCs of each WSI, quantified according to the six methods introduced in Sect. 2.2. The MCs quantified by the DFS are generally higher than those with rectangular or linear HPF arrangements: On average, DFS counted 4.29 and 3.32 additional mitoses than those with linear and rectangular HPF arrangements, respectively.

Importantly, our proposed DFS algorithm identified two borderline cases where the meningioma grades may be higher than the original WHO grades from the consensus conferences, based on the MC alone. Slide #5, previously signed-out as WHO grade 1 meningioma, could be upgraded to grade 2 due to the presence of 4 mitoses in the DFS-counted 10 consecutive HPFs. Slide #19 was signed-out as WHO grade 2 meningioma, but could be upgraded to grade 3 based on the DFS finding of 21 mitoses/10HPFs.

For all 19 WSIs, the MCs in maximum 10 (not connected) HPFs exceed the WHO grade 1/2 threshold. The MCs in the randomly selected 10 HPFs (average=1.18 mitoses/10HPFs) are approximately 16.1% lower than the average MC/10HPFs (average=1.37 mitoses/10HPFs), which indicates these two metrics are not always aligned.

Figure 4(c) displays the spatial distribution of mitosis locations in one example WSI (slide #11). It also shows the hotspot 10 HPFs identified by the DFS algorithm, and with linear/rectangular arrangements exhibiting roughly similar locations. Nonetheless, the MCs in these areas significantly differ due to the variation in HPF arrangements: the MC in the DFS-calculated HPFs was 19. However, the rectangular arrangement had 14, and the linear arrangement only had 9 or 11.

### Participants' correctness of detecting mitoses

Overall, the 41 participants achieved an average precision of 0.750 (Standard Deviation (*SD*) 0.026, 95% Confidence Interval (*CI95*) [0.698, 0.800]), sensitivity 0.667 (*SD* 0.002, *CI95* [0.626, 0.704]). Among the participants, the

(See figure on next page.)

**Fig. 4** **a** Example of annotated mitoses in the meningioma WSIs at different phases, including prophase, metaphase, anaphase-telophase, and atypical mitoses, bar=10 $\mu$ m. **b** Hotspot MC per 10 HPFs in each WSI using five methods of quantification, namely the proposed DFS algorithm, linear 10 HPFs (i.e., 10  $\times$  1 and 1  $\times$  10 arrangements), rectangular 10 HPFs (i.e., 5  $\times$  2 and 2  $\times$  5 arrangements), average MC per 10 HPFs, and maximum possible MC in 10 (not connected) HPFs. For the MC distribution in randomly-sampled 10 HPFs: the box-whisker plot shows the percentiles and medians, and the magenta error bars demonstrate the average and 95% confidence intervals. For each WSI, the WHO grade assigned at the consensus conference was included. **c** Mitosis distribution in slide #11, and the spatial distribution of 10 HPFs with the proposed DFS algorithm (MC=19), linear 10 HPFs (MC=9 or 11), and rectangular 10 HPFs (MC=14), bar=1mm



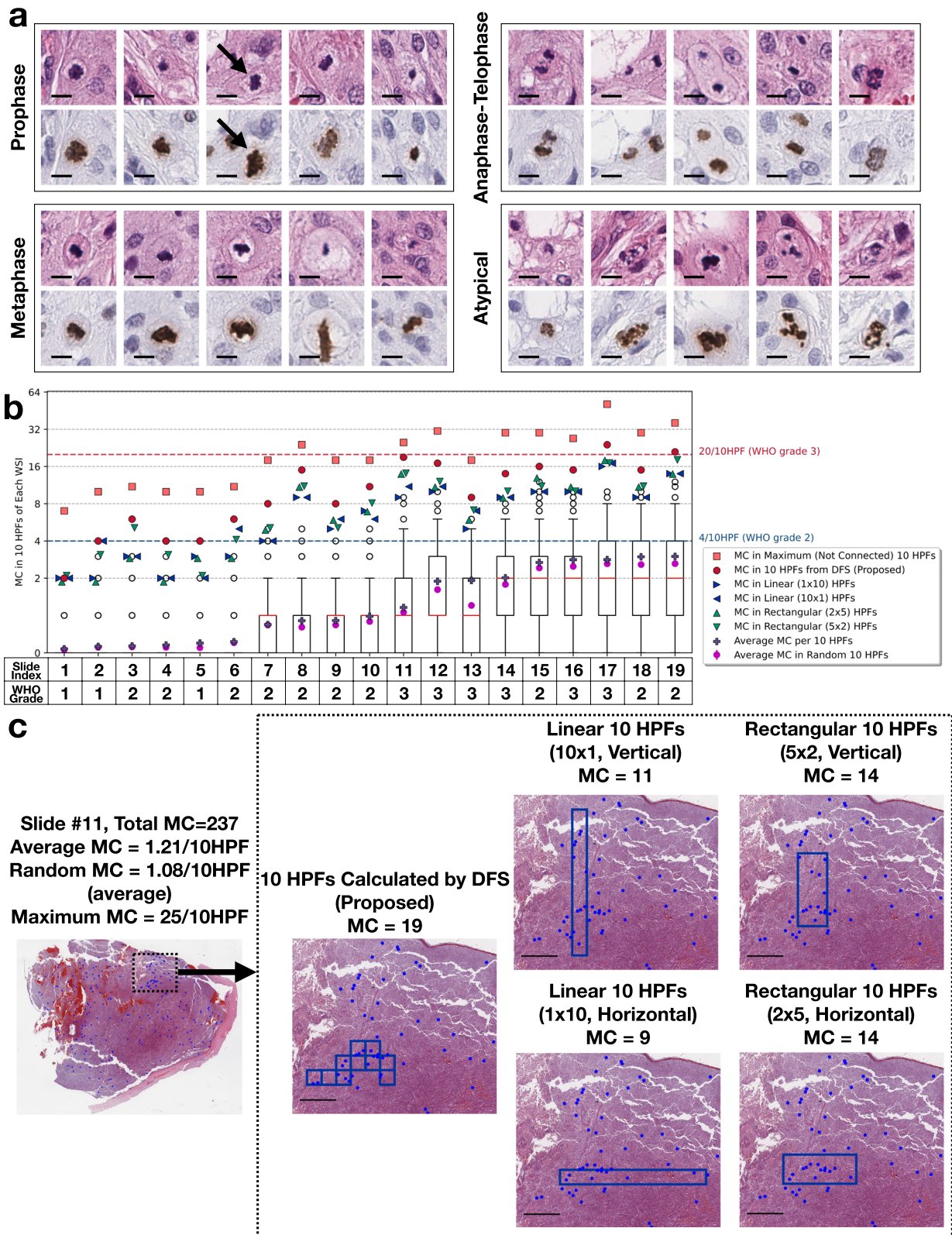


**Fig. 4** (See legend on previous page.)

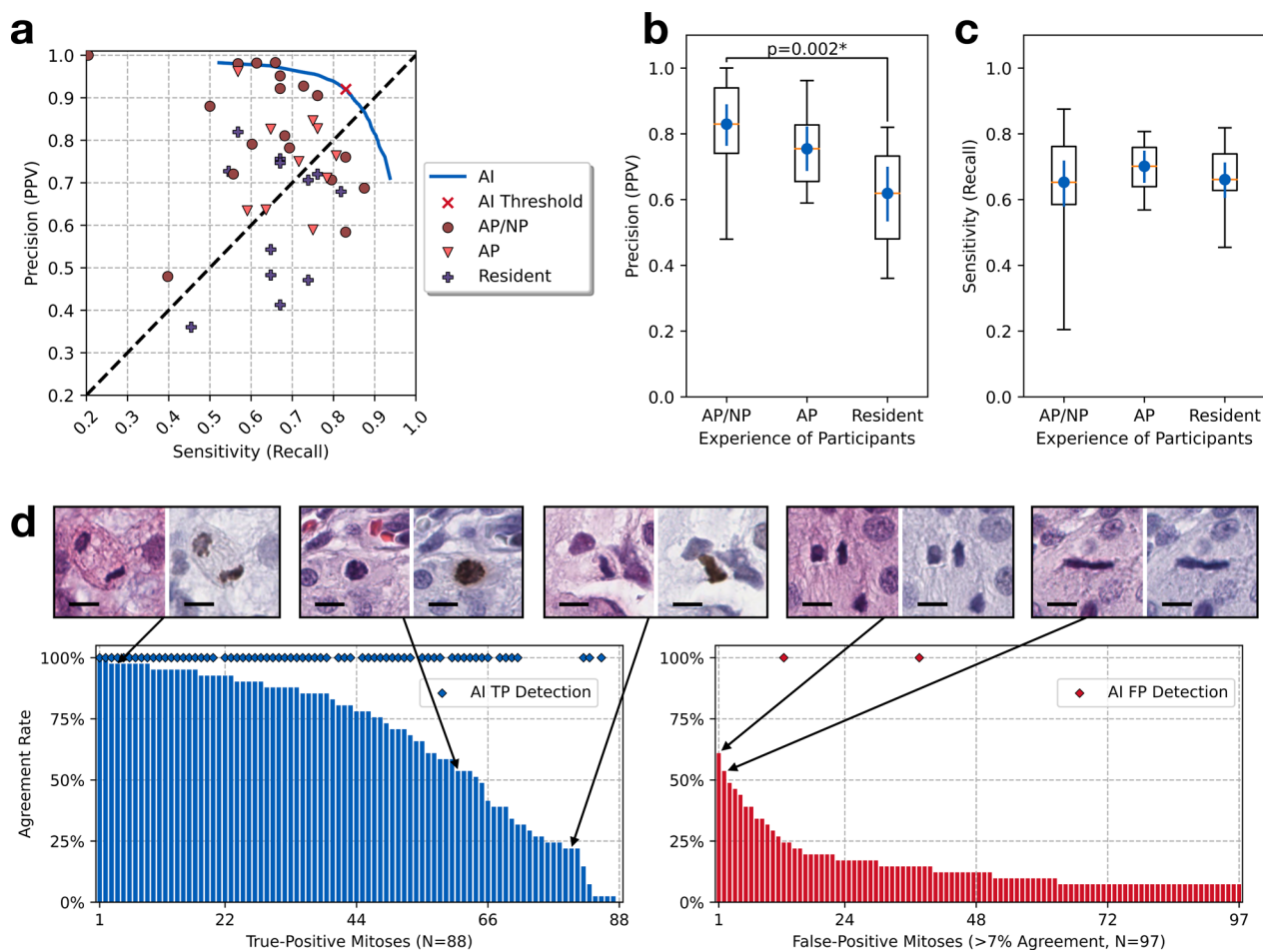


**Fig. 5** **a** The precision-recall scatter plot for each participant's performance in detecting mitoses on the 48 HPF images from the user study. The blue line indicates the precision-recall curve from AI and the marker (x) indicates AI's operating point with the threshold cut-off. The diagonal dashed line is the reference where the precision is equal to sensitivity. **b** The box-whisker plot with the average and 95% confidence interval, showing the precision (PPV) values of the participant groups with different experience levels: AP/NP, AP, and pathology residents. AP/NP participants achieved significantly higher precision than pathology residents ( $p=0.002$ , post-hoc Dunn's test). **c** Box-whisker plot with 95% confidence intervals, showing the sensitivity (recall) values of the participant groups with different experience levels. No statistical significance was observed. **d** Bar plots illustrating the agreement rates of participants in identifying ground-truth mitoses and false-positive mitoses, with selected examples (bar= $10\mu\text{m}$ ). The AI detections (both true-positive and false-positive) are shown as the diamond ( $\diamond$ ) markers

top-2<sup>3</sup> were a neuropathologist and a neuropathology fellow, achieving a tied score with a precision of 0.905 and a sensitivity of 0.761 (TP: 67, FP: 7, FN: 21). In contrast, the AI model achieved an average precision 0.920 ( $SD$  0.002,  $CI_{95}$  [0.916, 0.923]) and sensitivity 0.830 ( $SD$  0.002,  $CI_{95}$  [0.826, 0.833]). As shown in Fig. 5(a), the AI model exhibits both high precision and sensitivity, resulting a performance better than human participants.

Participants made significantly fewer false-positive mistakes than false-negative ones ( $p = 0.012$ , effect size  $r = 0.277$ , Wilcoxon rank sum test), indicating that they

tended to achieve a higher precision than a higher sensitivity: As shown in Fig. 5(a), 26 out of 41 participants achieved a higher precision than sensitivity (above the diagonal dashed line), while 15 out of 41 participants achieved a higher sensitivity instead (below the diagonal dashed line).

A Kruskal-Wallis test revealed a significant difference in participants' precision ( $p = 0.003$ ,  $\eta_H^2 = 0.231$ ) according to their experience level. Post-hoc Dunn's test indicated a significant difference ( $p = 0.002$ ) in the precision between AP/NP participants and pathology residents (Fig. 5(b)). The average precision of the former group was 0.829 ( $SD$  0.033,  $CI_{95}$  [0.763, 0.890]), while the latter had 0.619 ( $SD$  0.043,  $CI_{95}$  [0.531, 0.701]), indicating

<sup>3</sup> The top-2 is defined by the F1 score, which is the geometry mean of precision and sensitivity.

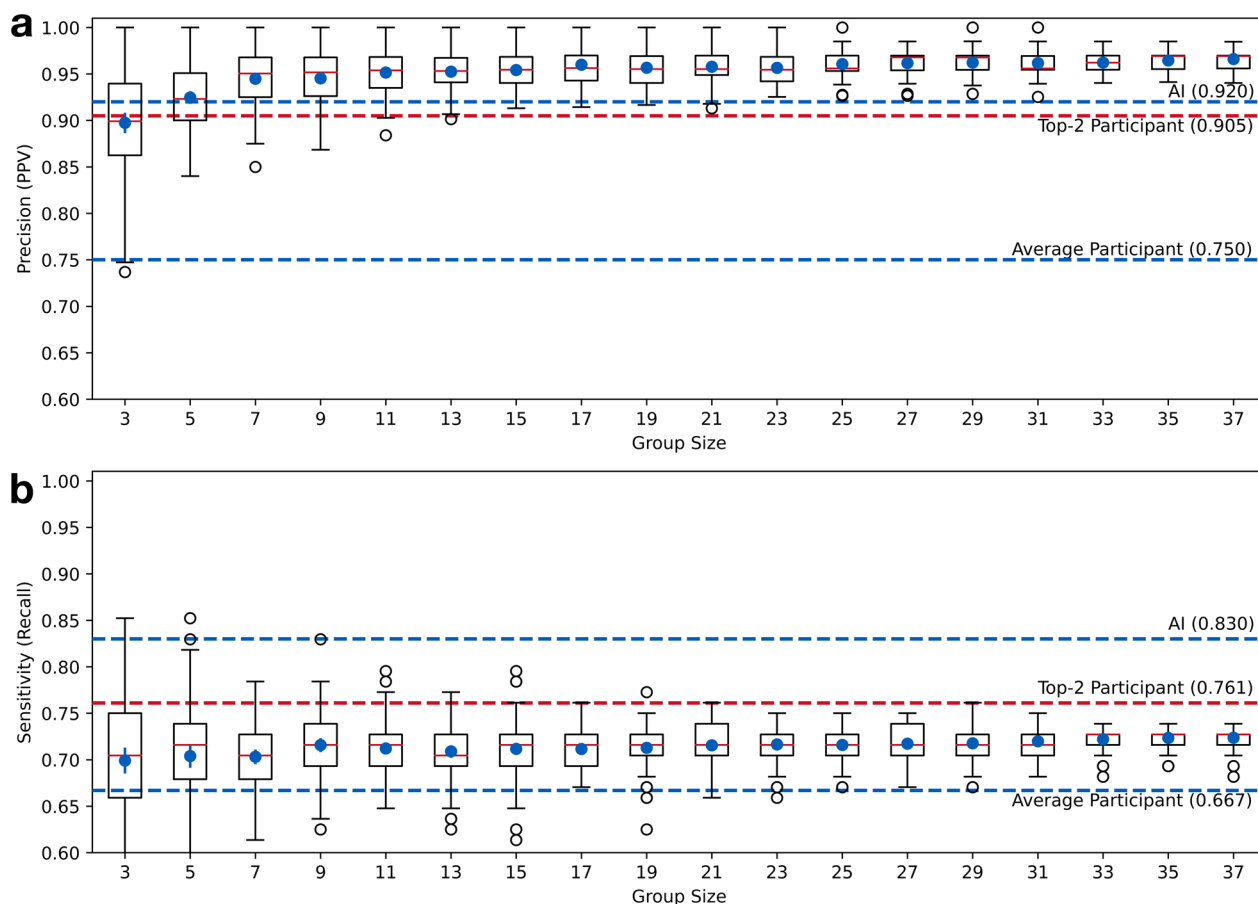


**Fig. 6** Box-whisker plot with the average and 95% confidence interval for **a** precision and **b** sensitivity values of decisions derived from grouped participants

a 33.93% increase. No significance was observed among other comparison pairs. As for the sensitivity (Fig. 5(c)), the Kruskal-Wallis test did not show a significance due to participants' experience level ( $p = 0.715$ ).

Figure 5(d) shows the distribution of participants' agreement rates for 88 ground-truth and 97 false-positive mitoses that at least three participants had agreed on. Among the ground-truth mitoses, 64 out of 88 had agreement rates exceeding 50%, while only 2 out of 97 false-positive mitoses achieved agreement rates above 50%. This provides motivations to use the majority voting approach to reduce false-positive errors.

**Grouping pathologists' decisions and evaluation of correctness**

Figure 6(a) presents the precision of decisions of groups sized between 3 and 37. The figure demonstrates that the grouping process can effectively mitigate random errors made by individual pathologists: Even groups of three participants achieved an average precision of 0.897

( $SD$  0.006,  $CI95$  [0.886, 0.908]). Compared to the precision an average participant (0.750), the groups of three participants demonstrated a 19.60% increase. Groups of five participants achieved an average precision of 0.925 ( $SD$  0.004,  $CI95$  [0.918, 0.932]), which was slightly higher than the AI model (0.920, 0.54% increase), and the top-2 individual participants (0.905, 2.21% increase). Groups of more than seven participants would have a higher precision in general, ranging from 0.945 (for groups of 7) to 0.966 (for groups of 37).

The average sensitivity of groups of three participants was 0.699 ( $SD$  0.007,  $CI95$  [0.685, 0.713]), which was also higher than an average participant (0.667, 4.79% increase). Figure 6(b) shows the sensitivity scores for groups of varying sizes, ranging from an average of 0.699 (for groups of 3) to 0.724 (for groups of 37). The sensitivities of grouped participants are lower the top-2 participants (0.761) and the AI model (0.830) in general.

Interestingly, the peak sensitivity of 0.852 was reached by a specific group of three participants, who also had a precision of 0.862. However, out of the 100 grouping



experiments that involved sampling three participants, we observed only two groups that outperformed AI in terms of sensitivity.

## Discussion

Mitosis is an important component in grading many brain tumors such as meningioma, IDH-mutant astrocytoma, oligodendroglioma, solitary fibrous tumor and ependymoma among others [2]. Additionally, mitosis can provide clues to modify a differential diagnosis toward a more accurate diagnosis. For instance, a subependymoma with few mitoses may prompt more careful examination for including an ependymoma-subependymoma in the differential [40]. Few scattered mitoses in a high-grade appearing IDH-wild type astrocytic tumor should add pleomorphic xanthoastrocytoma to the differential diagnosis beside glioblastoma usually demonstrating brisk mitotic activity [2]. Accurate mitosis quantification and detection is important but time-consuming – it can be challenging especially in large and heterogeneous specimens, where few highly proliferative foci, present in only one slide, are easily missed.

To our best knowledge, this is the first study to comprehensively analyze MC quantification approaches and observe the “grading migration” [41] through a new computer algorithm for mitoses counting. However, it should be underscored that the aim of the study is not highlighting the errors of pathologists. Instead, this work demonstrates the potential of using computer algorithms to precisely quantify MCs following the WHO guidelines. The algorithm can offer more flexibility in arranging HPFs, which may be challenging for human pathologists, even in digital interfaces. Furthermore, this study is also unique in its evaluation of pathologists’ ability for mitosis detection with the largest number of participants so far, compensating for previous studies that had limited participants and highlighted the inter-pathologist variation in detecting mitotic events [4, 24]. Because of its large participant size, this work demonstrates that a higher precision and more robust mitosis detection can actually be achieved by the majority voting from a group of pathologists.

While new molecular methods such as chromosomal microarray analysis [42], next generation sequencing [43], and methylation profiling [20] provide better understanding of tumor biology and behavior, they are time-consuming, costly and unavailable in many countries [44]. This technology gap generates an urgent need for developing AI-assisted solutions to analyze the mitotic count based on the histologic analysis. The AI pathology assistant is instantly present, cost-effective, and available 24/7, especially for institutions where trained neuropathologists are less available. In this study, for

example, the average time for pathologists to annotate the 48 HPF images was about 24 min 32 s ( $SD = 91.63$  seconds,  $CI_{95}=[21 \text{ min } 56 \text{ s}, 27 \text{ min } 55 \text{ s}]$ ). In contrast, it only took about 1 min 33 s ( $SD = 6.08$  seconds,  $CI_{95}=[1 \text{ min } 24 \text{ s}, 1 \text{ min } 41 \text{ s}]$ ) for a computer (see Sect. 2.5 for hardware configuration) to finish the mitosis detection by AI. It is noteworthy that such computer speed can be further accelerated by parallel computing, where clusters of computers split the task and work individually in parallel. In the future, the AI shall examine the entire set of slides, detect almost all mitotic figures, and generate a detailed report showing mitosis hotspots.

Since 2012, a considerable amount of literature has built mitosis datasets for AI development [30–34, 45], although there is still a lack of mitosis datasets in meningiomas. A widely-adopted approach for mitosis-detection AI includes two steps: an initial AI model screening potential candidates, followed by a step-2 for verification by AI [30, 31, 46, 47]. This work follows this approach and introduces the first mitosis AI specifically trained based on mitoses in meningiomas, and compares the correctness of mitosis detection between humans and AI through a user study of 41 participants. We discovered that the AI could outperform pathologists in sensitivity. Although few pathologists achieved higher precision, AI maintained high precision and sensitivity simultaneously, which contributed to a higher overall performance.

Although AI has demonstrated impressive performance, human-based quality assurance must be introduced: mitotic figures identified by AI still need to be checked for accuracy, especially in substandard samples with cautery and other processing artifacts. To demonstrate this workflow of human pathologists’ supervision of AI, we have designed and implemented a prototype that can integrate the computational approach proposed in this study.

Figure 7(a) illustrates the prototype’s functionality, where users can activate the “Show ROI Recommendation” (ROI: region of interest) feature to visualize hotspot areas quantified by the DFS algorithm. Users have control over the number of DFS-quantified hotspots displayed (ranging from 1 to 5) as well as the sensitivity setting of AI. Upon selecting a DFS-calculated hotspot for further examination, the system guides the user to examine each HPF within the hotspot at higher magnification (Fig. 7(b)), with AI-detected mitoses boxed by the system. The prototype assists pathologists in maintaining consistency in the selection of hotspot areas found by the DFS algorithm and also allows them to see potential mitoses marked by AI in the high-sensitivity setting. To achieve a high precision, one can let a group of pathologists examine the slide with the prototype independently. Therefore, the combined high sensitivity by AI and high precision by pathologists can ultimately achieve a higher

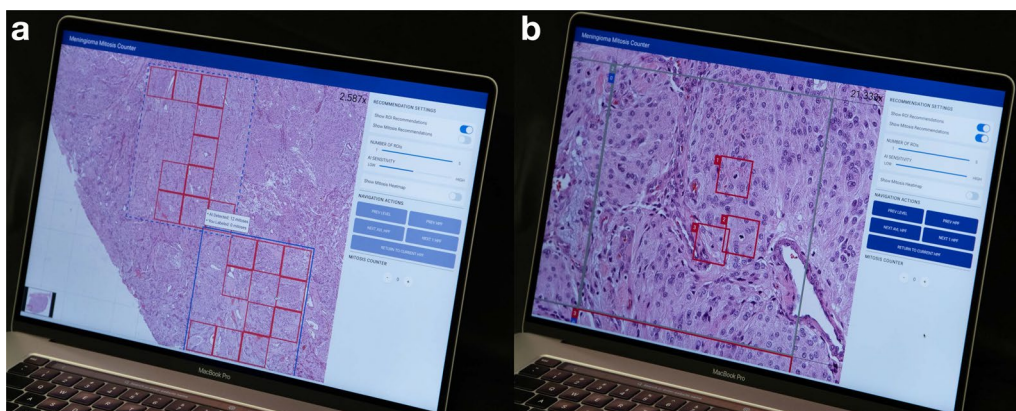


**Fig. 7** An AI-assisted prototype that conceptualizes the augmented pathology. **a** DFS-quantified mitosis hotspots are calculated based on AI-detected mitoses according to a sensitivity setting. The user can adjust the number of hotspots and adjust the AI sensitivity with the sliders on the right side of the interface. **b** Once a user selects a DFS-quantified hotspot, the prototype can guide the user to see each HPF inside, where it can mark a box surrounding each AI-detected mitosis candidate with the highest sensitivity. Multiple pathologists may visit the same hotspot areas recommended by the prototype to ensure the highest precision

overall performance. Even with AI as an assistant, it is the human pathologist who provides the adjudication for each mitosis, and mechanisms to prevent humans from blindly trusting AI should be introduced and evaluated in the future.

#### Limitations and future work

This work covers two aspects of mitosis quantification and mitosis detection. This subsection discusses the limitations in each aspect and suggests potential future directions for improvement.

For the experiment of the MC quantification:

1. *Cohort size* This study could have benefited by including other independent cohorts from different institutions, which need more resources not available at this time. To potentially address this, we extended the validation of the DFS algorithm to two additional public datasets with full-slide mitoses annotations in canine mammary carcinoma [31] and canine cutaneous mast cell tumors [30]. In both datasets, the DFS algorithm consistently demonstrated an ability to yield higher MCs compared to linear (~13 more) and rectangular (~8 more) HPF arrangements (see, Additional file 1 Section 6). While these results should not be directly compared to meningiomas due to varying mitosis prevalence rates across different tumor types, this preliminary finding sheds light on the potential of the DFS algorithm to enhance the MC quantification in various tumor contexts, providing a foundation for future large-cohort studies.
2. *Selection of slides* In this study, only one to two slides were sampled from each patient, which could inevita-

bly introduce bias to the MC quantification and subsequent grading analyses, because other slides might have a higher mitotic rate. Ideally, at least one tissue section/block/slide is recommended for every tumor cm. Therefore, future studies can include entire set of slides from each patient to ensure a comprehensive analysis.

For the user study evaluating the mitosis detection:

1. *Limited test images* The use of only 48 selected HPF images in the user study introduces potential biases and may influence the findings, and the duration of the study is relatively brief (about 30 min in total). Since pathologists are used to the H&E stain in their own institutions, they usually need more time to get used to H&E slides from another institution with different performance. Therefore, future work can focus on measuring pathologists' mitosis identification with more images from multi-z-axes WSIs and standardized H&E stains.
2. *One z-plane in WSI scanning* All specimens were scanned with only one z-plane instead of multiple, due to the limitation of instrumentation. In light microscopy, pathologists can adjust the z-focus, which can aid in judging the authenticity of a mitosis. Hence, the missing z-axis might cause pathologists to achieve a lower sensitivity, which, unfortunately, makes the sensitivity values reported in this work inevitably speculative.
3. *Generalizability of AI* The AI used in this study was developed based on a single meningioma dataset, and the bench-marking of its performance on other

tumor datasets is, unfortunately, out of the scope of this study and thus considered as future work.

4. *Participant selection* There was also a potential bias in the participants, because the majority of participants are from the United States. To address this, we have provided public access to the user study website (<https://mg-labeler.vercel.app>) and encourage readers of interest to participate.

## Conclusion

This work presents a computational strategy that leverages digital pathology to enhance the quantification and detection of mitosis. The strategy consists of two key components: (1) a depth-first search algorithm that quantifies the mathematical maximum mitosis count in 10 consecutive HPFs, enabling more precise grading, especially in cases with borderline mitotic figures; and (2) a collaborative approach that groups pathologists to detect mitoses under each HPF, reducing random errors from individual assessments and thus increasing assessment robustness. The integration of our computational strategy with AI promises a more efficient and robust mitosis assessment by pathologists, which holds the potential to create more accurate

reports when mitoses count is critical for tumor grading, and ultimately, benefits patient management.

## Appendix A depth-first search algorithm to calculate sum of mitosis count in highest 10 consecutive HPFs

Locations of all mitosis annotations (whether they were annotated by pathologists or detected by AI) of a WSI are needed in order to run the DFS algorithm. Firstly, the WSI was split into non-overlapping HPF tiles. Then, a matrix of MC for each HPF in the WSI, denoted as *WSI*, was built. The coordinate of each element in *WSI* matrix represents the location of a HPF, and the value represents the MC in this HPF. The algorithm `FindMaxMC` is the main function, and algorithm `Search` is the helper function. To calculate with DFS, the *WSI* matrix should be passed to `FindMaxMC` function, and it will return two values: (1) *maxSum*: the highest MC in 10 consecutive HPFs, and (2) *maxPath*: the locations of these 10 HPFs.

**Algorithm 1** Find the max MC in 10 consecutive HPFs of a WSI

---

```

1 Function FindMaxMC(WSI):
2   maxSumWSI ← 0    // stores the max MC of the max path in a
   WSI
3   maxPathWSI ← Nul    // stores locations of HPFs in the max
   path
4   for i from 0 to RowCount(WSI) - 1 do
5     for j from 0 to ColumnCount(WSI) - 1 do
6       /* for each HPF in a WSI (in each column and each row),
7         find a path of 10 HPFs that starts from this exact
8         HPF and has the highest MC) */
9       sum, path ← Search(WSI, WSI[i][j], [(i, j)])
10      if sum > maxSum then
11        /* update the highest MC and max path if a path with
12        a higher MC was found) */
13        maxSumWSI ← sum
14        maxPathWSI ← path
15  return maxSum, maxPath

```

---

**Algorithm 2** Depth-first search helper function

```

1 Function Search(WSI, sum, path):
2   if length(path) = 10 then
3     /* return if the length of the path is equal to 10 (10
4       HPFs) */
5     return sum, path
6   maxSum ← 0 // stores the max MC of the max path
7   maxPath ← Nil // stores locations of HPFs in the max path
8   for dx, dy in [(0,1), (0,-1), (1,0), (-1,0)] do
9     x ← path[-1][0] + dx
10    y ← path[-1][1] + dy
11    /* find the location of the last HPF in the current path,
12      and search its connected neighbors (top, bottom, left,
13      right) */
14    if WSI[x][y] is valid and (x, y) ∉ path then
15      /* if the neighbor is within the limit of WSI, and the
16        neighbor is not in the current path */
17      nextSum, nextPath ← Search(WSI, sum + WSI[x][y], path ∪ (x,
18        y)) // acquire the MC and locations of the new path
19        (with the added neighbor)
20      if nextSum > maxSum then
21        /* update the max MC and HPF locations of the max
22          path if the new path (with the added neighbor) has
23          a higher MC */
24        maxSum ← nextSum
25        maxPath ← nextPath

```

**Appendix B summary of participants’ affiliations**

See Table 1

**Table 1** Participants’ affiliations in the user study

| Institution                                   | Number of Participants |
|---|------------------------|
| Kansas University Medical Center              | 18                     |
| UCLA / Ronald Reagan UCLA Medical Center      | 6                      |
| Baylor College of Medicine / Texas Children’s | 6                      |
| Brown University / Rhode Island Hospital      | 3                      |
| University of California, San Francisco       | 1                      |
| Mayo Clinic                                   | 1                      |
| University of Pennsylvania / Penn Medicine    | 1                      |
| USC / Los Angeles General Medical Center      | 1                      |
| Loma Linda University                         | 1                      |
| UTHealth Houston                              | 1                      |
| Other (Unspecified / not in United States)    | 2                      |
| Total   | 41                     |

**Abbreviations**

|                     |  |
|---------------------|--|
| CNS                 | Central nervous system   |
| WHO                 | World Health Organization                                      |
| WHO CNS 5 Blue Book | The 2021 WHO classification of tumors of the CNS (5th edition) |
| MC                  | Mitotic count  |
| IHC                 | Immunohistochemistry   |
| PHH3                | Phosphohistone-H3  |
| AI                  | Artificial intelligence  |
| WSI                 | Whole slide image  |
| HPF                 | High-power field   |
| DFS                 | Depth-first search   |
| AP/NP               | Neuropathologists/neuropathology fellows                       |
| AP                  | Pathologists/pathology fellow                                  |
| TP                  | True-positive  |
| FP                  | False-positive   |
| FN                  | False-negative   |
| SD                  | Standard deviation   |
| CI95                | 95% Confidence interval  |
| ROI                 | Region of interest   |

## Supplementary Information

The online version contains supplementary material available at <https://doi.org/10.1186/s40478-023-01707-6>.

**Additional file 1:** Summary of supplementary documents.

**Additional file 2:** De-identified information sheet of mitosis count summary for each WSI.

**Additional file 3:** Mitosis count in 10 HPFs with the DFS, linear, and rectangular arrangements, with regard to the shift in the coordinate origins.

**Additional file 4:** Mitosis annotations (ground truth) of the 48 HPF images in the user study.

**Additional file 5:** Performance report of a typical AI prediction on the 48 HPF images.

**Additional file 6:** Performance report of the top-2 participants that achieved the best performance in the user study (1/2).

**Additional file 7:** Performance report of the top-2 participants that achieved the best performance in the user study (2/2).

### Acknowledgements

We appreciate the anonymous pathologists who participated in this research.

### Author contributions

Conceptualization and Design – Pathology: M.H., H.V.V. Conceptualization and Design – Data Analysis and User Study: M.H., H.G., X.A.C. Data Acquisition – Pathology: I.A.-K., N.L., C.K.W., S.M.A., E.K.O., C.Y., N.K., I.C., N.Z.-K., X.R.Z. Data Acquisition – Software: C.Y., H.G. Data Acquisition – User Study Coordination: N.Z.-K., M.H. Data Analysis and Visualization: H.G., M.H., X.A.C. Writing – Draft Preparation: H.G., M.H., X.A.C., W.Y. Writing – Review and Editing: M.H., H.V.V., X.A.C., S.M. All authors read and approved the final manuscript.

### Funding

This work is funded partly by the University of Kansas start-up fund to Mohammad Haeri, and the National Science Foundation of the United States (IIS-1850183).

### Availability of data and materials

The user study website can be accessed publicly online. The mitoses annotations of the images used in the user study, a summary information sheet of mitosis count for each Whole Slide Image, reports of the AI's and top-2 participants' performance in the user study are also submitted as the supplementary material. Other raw data generated from the study are available from the corresponding authors upon reasonable request.

### Declarations

#### Conflict of interest

Authors declare no conflict of interest.

#### Ethics approval and consent to participate

The user study was approved by the Institutional Review Board of the University of California, Los Angeles (IRB#21-000139). All pathologist/pathology resident participants gave consent to participate in this study.

#### Consent for publication

Not applicable.

#### Author details

<sup>1</sup>Electrical and Computer Engineering, University of California, Los Angeles, Los Angeles, CA 90095, USA. <sup>2</sup>Pathology and Laboratory Medicine, The University of Kansas Medical Center, Kansas City, KS 66160, USA. <sup>3</sup>Pathology and Laboratory Medicine, UCLA David Geffen School of Medicine, Los Angeles, CA 90095, USA. <sup>4</sup>Department of Pathology, Stanford Medical School, Stanford, CA 94305, USA. <sup>5</sup>McGovern Medical School, UT Health at Houston, Houston, TX 77030, USA. <sup>6</sup>Baylor College of Medicine, Houston, TX 77030, USA.

Received: 24 October 2023 Accepted: 10 December 2023

Published online: 11 January 2024

### References

- Ostrom QT, Price M, Neff C, Cioffi G, Waite KA, Kruchko C, et al. (2022) CBTRUS Statistical Report: Primary Brain and Other Central Nervous System Tumors Diagnosed in the United States in 2015–2019. *Neuro-Oncology*. 10;24(Supplement\_5):v1–v95. [https://doi.org/10.1093/neuro-onc/2022.10.24.Supplement\\_5/v1/46359484/2022](https://doi.org/10.1093/neuro-onc/2022.10.24.Supplement_5/v1/46359484/2022). [https://academic.oup.com/neuro-oncology/article-pdf/24/Supplement\\_5/v1/46359484/2022.pdf](https://academic.oup.com/neuro-oncology/article-pdf/24/Supplement_5/v1/46359484/2022.pdf)
- Louis DN, Perry A, Wesseling P, Brat DJ, Cree IA, Figarella-Branger D et al (2021) The 2021 WHO classification of tumors of the central nervous system: a summary. *Neuro Oncol* 23(8):1231–1251. <https://doi.org/10.1093/neuonc/noab106>
- Bertram CA, Aubreville M, Gurtner C, Bartel A, Corner SM, Dettwiler M et al (2020) Computerized calculation of mitotic count distribution in canine cutaneous mast cell tumor sections: mitotic count is area dependent. *Vet Pathol* 57(2):214–226. <https://doi.org/10.1177/0300985819890686>
- Meyer JS, Alvarez C, Milikowski C, Olson N, Russo I, Russo J et al (2005) Breast carcinoma malignancy grading by Bloom–Richardson system vs proliferation index: reproducibility of grade and advantages of proliferation index. *Mod Pathol* 18(8):1067–1078. <https://doi.org/10.1038/modpathol.3800388>
- Collan YU, Kuopio T, Baak JPA, Becker R, Bogomoletz WV, Devereil M et al (1996) Standardized mitotic counts in breast cancer evaluation of the method. *Pathol Res Pract* 192(9):931–941. [https://doi.org/10.1016/S0344-0338\(96\)80075-6](https://doi.org/10.1016/S0344-0338(96)80075-6)
- Garcia CR, Slone SA, Dolecek TA, Huang B, Neltner JH, Villano JL (2019) Primary central nervous system tumor treatment and survival in the United States, 2004–2015. *J Neurooncol* 144(1):179–191. <https://doi.org/10.1007/s11060-019-03218-8>
- Cree IA, Tan PH, Travis WD, Wesseling P, Yagi Y, White VA et al (2021) Counting mitoses: SI(ze) matters! *Mod Pathol* 34(9):1651–1657. <https://doi.org/10.1038/s41379-021-00825-7>
- Goldbrunner R, Stavrinou P, Jenkinson MD, Sahm F, Mawrin C, Weber DC et al (2021) EANO guideline on the diagnosis and management of meningiomas. *Neuro Oncol* 23(11):1821–1834. <https://doi.org/10.1093/neuonc/noab150>
- Ohta M, Iwaki T, Kitamoto T, Takeshita I, Tateishi J, Fukui M (1994) MIB1 staining index and scoring of histologic features in meningioma. Indicators for the prediction of biologic potential and postoperative management. *Cancer* 74(12):3176–3189. [https://doi.org/10.1002/1097-0142\(19941215\)74:12<3176::AID-CNCR2820741217>3.0.CO;2-N](https://doi.org/10.1002/1097-0142(19941215)74:12<3176::AID-CNCR2820741217>3.0.CO;2-N)
- Abry E, Thomassen IØ, Salvesen ØO, Torp SH (2010) The significance of Ki-67/MIB-1 labeling index in human meningiomas: a literature study. *Pathol Res Pract* 206(12):810–815. <https://doi.org/10.1016/j.prp.2010.09.002>
- Liu N, Song SY, Jiang JB, Wang TJ, Yan CX (2020) The prognostic role of Ki-67/MIB-1 in meningioma: a systematic review with meta-analysis. *Medicine* 99(9):e18644. <https://doi.org/10.1097/MD.00000000000018644>
- Harter PN, Braun Y, Plate KH (2017) Classification of meningiomas—advances and controversies. *Chin Clin Oncol* 6(S1):S2–S2. <https://doi.org/10.21037/cco.2017.05.02>
- Hendzel MJ, Wei Y, Mancini MA, Van Hooser A, Ranalli T, Brinkley BR et al (1997) Mitosis-specific phosphorylation of histone H3 initiates primarily within pericentromeric heterochromatin during G2 and spreads in an ordered fashion coincident with mitotic chromosome condensation. *Chromosoma* 106(6):348–360. <https://doi.org/10.1007/s004120050256>
- Duregon E, Cassenti A, Pittaro A, Ventura L, Senetta R, Rudà R et al (2015) Better see to better agree: phosphohistone H3 increases interobserver agreement in mitotic count for meningioma grading and imposes new specific thresholds. *Neuro Oncol* 17(5):663–669. <https://doi.org/10.1093/neuonc/nov002>. (02)



15. Ribalta T, McCutcheon IE, Aldape KD, Bruner JM, Fuller GN (2004) The mitosis-specific antibody anti-phosphohistone-H3 (PHH3) facilitates rapid reliable grading of meningiomas according to WHO 2000 criteria. *Am J Surg Pathol* 28(11):1532–1536. <https://doi.org/10.1097/01.pas.0000141389.06925.d5>
16. Kim YJ, Ketter R, Steudel WI, Feiden W (2007) Prognostic significance of the mitotic index using the mitosis marker anti-phosphohistone H3 in meningiomas. *Am J Clin Pathol* 128(1):118–125. <https://doi.org/10.1309/HXUNAG34B3CEFDU8>
17. Fukushima S, Terasaki M, Sakata K, Miyagi N, Kato S, Sugita Y et al (2009) Sensitivity and usefulness of anti-phosphohistone-H3 antibody immunostaining for counting mitotic figures in meningioma cases. *Brain Tumor Pathol* 26:51–57. <https://doi.org/10.1007/s10014-009-0249-9>
18. Singh J, Sharma R, Shukla N, Narwal P, Katiyar A, Mahajan S et al (2023) DNA methylation profiling of meningiomas highlights clinically distinct molecular subgroups. *J Neurooncol* 161(2):339–356. <https://doi.org/10.1007/s11060-022-04220-3>
19. Nassiri F, Mamatjan Y, Suppiah S, Badhiwala JH, Mansouri S, Karimi S et al (2019) DNA methylation profiling to predict recurrence risk in meningioma: development and validation of a nomogram to optimize clinical management. *Neuro Oncol* 21(7):901–910. <https://doi.org/10.1093/neuonc/noz061>
20. Capper D, Stichel D, Sahm F, Jones DTW, Schrimpf D, Sill M et al (2018) Practical implementation of DNA methylation and copy-number-based CNS tumor diagnostics: the Heidelberg experience. *Acta Neuropathol* 136(2):181–210. <https://doi.org/10.1007/s00401-018-1879-y>
21. Sahm F, Schrimpf D, Stichel D, Jones DTW, Hielscher T, Schefzyk S et al (2017) DNA methylation-based classification and grading system for meningioma: a multicentre, retrospective analysis. *Lancet Oncol* 18(5):682–694. [https://doi.org/10.1016/S1470-2045\(17\)30155-9](https://doi.org/10.1016/S1470-2045(17)30155-9)
22. Wang JZ, Nassiri F, Aldape K, von Deimling A, Sahm F (2023) The epigenetic landscape of meningiomas. *Adv Exp Med Biol* 1416:175–188. [https://doi.org/10.1007/978-3-031-29750-2\\_13](https://doi.org/10.1007/978-3-031-29750-2_13)
23. Aubreville M, Bertram CA, Marzahl C, Gurtner C, Dettwiler M, Schmidt A et al (2020) Deep learning algorithms out-perform veterinary pathologists in detecting the mitotically most active tumor region. *Sci Rep* 10(1):16447. <https://doi.org/10.1038/s41598-020-73246-2>
24. Veta M, Van Diest PJ, Jiwa M, Al-Janabi S, Pluim JPW (2016) Mitosis counting in breast cancer: object-level interobserver agreement and comparison to an automatic method. *PLoS ONE* 11(8):e0161286. <https://doi.org/10.1371/journal.pone.0161286>
25. Gu H, Yang C, Haeri M, Wang J, Tang S, Yan W, et al. (2023) Augmenting Pathologists with NaviPath: Design and Evaluation of a Human-AI Collaborative Navigation System. In: Proceedings of the 2023 CHI conference on human factors in computing systems. CHI '23. New York: Association for Computing Machinery. Available from: <https://doi.org/10.1145/3544548.3580694>
26. Gu H, Liang Y, Xu Y, Williams CK, Magaki S, Khanlou N et al (2023) Improving workflow integration with XPath: design and evaluation of a human-ai diagnosis system in pathology. *ACM Trans Comput-Hum Interact*. <https://doi.org/10.1145/3577011>
27. Bertram CA, Aubreville M, Donovan TA, Bartel A, Wilm F, Marzahl C et al (2022) Computer-assisted mitotic count using a deep learning-based algorithm improves interobserver reproducibility and accuracy. *Vet Pathol* 59(2):211–226. <https://doi.org/10.1177/03009858211067478>
28. Van Bergeijk SA, Stathonikos N, Ter Hoeve ND, Lafarge MW, Nguyen TQ, Van Diest PJ et al (2023) Deep learning supported mitoses counting on whole slide images: a pilot study for validating breast cancer grading in the clinical workflow. *J Pathol Inform* 14:100316. <https://doi.org/10.1016/j.jpi.2023.100316>
29. Balkenhol MCA, Tellez D, Vreuls W, Clahsen PC, Pinckaers H, Ciompi F et al (2019) Deep learning assisted mitotic counting for breast cancer. *Lab Invest* 99(11):1596–1606. <https://doi.org/10.1038/s41374-019-0275-0>
30. Bertram CA, Aubreville M, Marzahl C, Maier A, Klopfeisch R (2019) A large-scale dataset for mitotic figure assessment on whole slide images of canine cutaneous mast cell tumor. *Sci Data* 6(1):274. <https://doi.org/10.1038/s41597-019-0290-4>
31. Aubreville M, Bertram CA, Donovan TA, Marzahl C, Maier A, Klopfeisch R (2020) A completely annotated whole slide image dataset of canine breast cancer to aid human breast cancer research. *Sci Data* 7(1):417. <https://doi.org/10.1038/s41597-020-00756-z>
32. Roux L, Racoceanu D, Loménié N, Kulikova M, Irshad H, Klossa J et al (2012) Mitosis detection in breast cancer histological images an ICPR 2012 contest. *J Pathol Inform* 4(1):8. <https://doi.org/10.4103/2153-3539.112693>
33. Veta M, Heng YJ, Stathonikos N, Bejnordi BE, Beca F, Wollmann T et al (2019) Predicting breast tumor proliferation from whole-slide images: the TUPAC16 challenge. *Med Image Anal* 54:111–121. <https://doi.org/10.1016/j.media.2019.02.012>
34. Aubreville M, Stathonikos N, Bertram CA, Klopfeisch R, ter Hoeve N, Ciompi F et al (2023) Mitosis domain generalization in histopathology images—the MIDOG challenge. *Med Image Anal* 84:102699. <https://doi.org/10.1016/j.media.2022.102699>
35. Stacke K, Eilertsen G, Unger J, Lundstrom C (2021) Measuring domain shift for deep learning in histopathology. *IEEE J Biomed Health Inform* 25(2):325–336. <https://doi.org/10.1109/JBHI.2020.3032060>
36. Aubreville M, Bertram C, Veta M, Klopfeisch R, Stathonikos N, Breininger K, et al. (2021) Quantifying the scanner-induced domain gap in mitosis detection. arXiv preprint [arXiv:2103.16515](https://arxiv.org/abs/2103.16515)
37. Wang Z, Hosseini MS, Miles A, Plataniotis KN, Wang Z (2020) FocusLiteNN: high efficiency focus quality assessment for digital pathology. In: Martel AL, Abolmaesumi P, Stoyanov D, Mateus D, Zuluaga MA, Zhou SK et al (eds) Medical image computing and computer assisted intervention - MICCAI 2020. Springer International Publishing, Cham
38. Gu H, Haeri M, Ni S, Williams CK, Zarrin-Khameh N, Magaki S, et al. (2023) Detecting Mitoses with a Convolutional Neural Network for MIDOG 2022 Challenge. In: Mitosis domain generalization and diabetic retinopathy analysis: MICCAI challenges MIDOG 2022 and DRAC 2022, Held in Conjunction with MICCAI 2022, Singapore, Sept 18–22, 2022, Proceedings. Springer-Verlag, Berlin p. 211–216. Available from: [https://doi.org/10.1007/978-3-031-33658-4\\_21](https://doi.org/10.1007/978-3-031-33658-4_21)
39. Tan M, Le Q (2019) EfficientNet: Rethinking model scaling for convolutional neural networks. In: Chaudhuri K, Salakhutdinov R, eds. Proceedings of the 36th international conference on machine learning. vol. 97 of Proceedings of machine learning research. PMLR. pp. 6105–6114. Available from: <https://proceedings.mlr.press/v97/tan19a.html>
40. Scheithauer BW (1978) Symptomatic subependymoma. Report of 21 cases with review of the literature. *J Neurosurg* 49(5):689–696. <https://doi.org/10.3171/jns.1978.49.5.689>
41. Feinstein AR, Sosin DM, Wells CK (1985) The Will Rogers phenomenon: stage migration and new diagnostic techniques as a source of misleading statistics for survival in cancer. *N Engl J Med* 312(25):1604–1608. <https://doi.org/10.1056/NEJM198506203122504>
42. Mischel PS, Cloughesy TF, Nelson SF (2004) DNA-microarray analysis of brain cancer: molecular classification for therapy. *Nat Rev Neurosci* 5(10):782–792. <https://doi.org/10.1038/nrn1518>
43. Sahm F, Schrimpf D, Jones DT, Meyer J, Kratz A, Reuss D et al (2016) Next-generation sequencing in routine brain tumor diagnostics enables an integrated diagnosis and identifies actionable targets. *Acta Neuropathol* 131(6):903–910. <https://doi.org/10.1007/s00401-015-1519-8>
44. Kurdyukov S, Bullock M (2016) DNA methylation analysis: choosing the right method. *Biology*. <https://doi.org/10.3390/biology5010003>
45. Aubreville M, Wilm F, Stathonikos N, Breininger K, Donovan TA, Jabari S et al (2023) A comprehensive multi-domain dataset for mitotic figure detection. *Sci Data* 10(1):484. <https://doi.org/10.1038/s41597-023-02327-4>
46. Sohail A, Khan A, Wahab N, Zameer A, Khan S (2021) A multi-phase deep CNN based mitosis detection framework for breast cancer histopathological images. *Sci Rep* 11(1):6215. <https://doi.org/10.1038/s41598-021-85652-1>
47. Mahmood T, Arsalan M, Owais M, Lee MB, Park KR (2020) Artificial intelligence-based mitosis detection in breast cancer histopathology images using faster R-CNN and deep CNNs. *J Clin Med* 9(3):749. <https://doi.org/10.3390/jcm9030749>

## Publisher's Note

Springer Nature remains neutral with regard to jurisdictional claims in published maps and institutional affiliations.